A Unified Control Strategy for Voltage Regulation and Congestion Management in Active Distribution Networks

Kalliopi D. Pippi, *Student Member, IEEE,* Georgios C. Kryonidis, *Member, IEEE,* Angelos I. Nousdilis, *Student Member, IEEE,* and Theofilos A. Papadopoulos, *Senior Member, IEEE*

***Abstract*—The advent of distributed renewable energy sources (DRESs) has led to a series of technical issues affecting the secure and reliable operation of active distribution networks. Among them, under-/overvoltages, current overload, and voltage unbalance can be considered as the most important problems limiting the increase of DRES penetration. In this paper, a new control architecture is proposed to overcome these issues using the reactive power of DRESs and the active/reactive power of distributed battery energy storage systems (DBESSs). Its distinct feature is the implementation in the symmetrical components domain, allowing the efficient decoupling between under-/overvoltage and voltage unbalance mitigation techniques. Furthermore, a central controller is introduced to improve the system performance in terms of reduced network losses and effective DBESS utilization by coordinating the response of DRESs and DBESSs. The validity of the proposed control strategy is evaluated by performing time-domain and time-series simulations on the IEEE European LV test feeder.**

***Index Terms*—Battery energy storage systems, congestion management, distributed renewable energy sources, voltage regulation, voltage unbalance mitigation.**

I. Introduction

DRIVEN by the proliferation of distributed renewable energy sources (DRESs), distribution networks have faced a transition from passive to active operation, introducing a new era to the electrical grid [1]. Nevertheless, this era has brought new challenges that distribution system operators (DSOs) should address to achieve higher DRES penetration levels and meet the final goal of a climate-neutral Europe by 2050 [2]. Among them, special consideration should be given to the following issues [3]: (a) under-/overvoltages, (b) voltage unbalance, and (c) current overload. Focusing on low-voltage (LV) distribution networks, these problems can be tackled by the combined operation of DRESs and DBESSs [4]; in such a case, the grid-interfaced converters control the active/reactive power output as well as the power allocation among the three-phases.

The research work was supported by the Hellenic Foundation for Research and Innovation (H.F.R.I.) under the "First Call for H.F.R.I. Research Projects to support Faculty members and Researchers and the procurement of high-cost research equipment grant" (Project Number: HFRI-FM17-229).

K. D. Pippi and T. A. Papadopoulos are with the Power Systems Laboratory, Department of Electrical and Computer Engineering, Democritus University of Thrace, Xanthi 67100, Greece (e-mail: kpippi@ee.duth.gr; thpapad@ee.duth.gr).

G. C. Kryonidis and A. I. Nousdilis are with the School of Electrical and Computer Engineering, Aristotle University of Thessaloniki, Thessaloniki 54124, Greece (e-mail: kryonidi@ece.auth.gr; angelos@auth.gr).

In literature, several solutions have been proposed to tackle voltage violations. More specifically, a consensus control scheme is presented in [5] where the active power of DBESSs is used to control network voltages. The use of the reactive power of DRESs and DBESSs as the only means for voltage regulation (VR) is assessed in [6] and [7] by developing distributed and centrally coordinated implementations, respectively. Nevertheless, the performance of these methods is limited since they don't fully exploit the controllability potential that can be provided by the combined use of active and reactive power. This is addressed in [8] by proposing a decentralized, droop-based method where the active power of DBESSs is combined with the reactive power of DRESs to control the network voltages. However, active power is prioritized against reactive power increasing the DBESSs utilization and deteriorating their lifetime expectancy. This priority is reversed in [9] where a consensus-based distributed control scheme is employed to coordinate the response of DRESs. Another promising solution is the use of centralized control schemes where the operating points of DRESs and DBESSs are determined using optimization techniques [10], [11] or rule-based [12] approaches. However, these methods assume balanced networks, which is unrealistic for LV distribution networks.

The unbalanced grid operation is considered in the VR algorithms developed in [13]–[16]. In particular, in [13], a consensus algorithm is proposed controlling the active power of DRESs and DBESSs at each phase separately. Similar approaches are presented in [14] and [15] where distributed algorithms are employed to control the output power of DRESs and DBESSs. A decentralized solution is presented in [16] where single-phase droop curves are introduced to tackle voltage violations. As a common drawback, these methods control the phase-to-neutral voltages which is not compliant with the regulation of the positive-sequence voltage imposed by the recently revised IEEE 1547 Standard [17]. Additionally, a strong coupling between voltage unbalance and positive-sequence voltage is introduced, hindering the individual handling.

Considering voltage unbalance mitigation (VUM), an extended version of the Steinmetz design is proposed in [18] where the zero- and/or negative-sequence voltages at critical network nodes are eliminated by properly adjusting the reactive power of DRESs among the three-phases. Although this method is valid, continuous monitoring of the unbalanced

loading conditions is needed, while the impact on the positive-sequence voltages is not assessed. In [19]–[21], an alternative VUM technique involves the use of the damping conductance concept enabling DRESs to behave as a constant shunt resistance in the zero- and negative-sequence. Moreover, the damping conductance concept is combined with a droop curve to address potential overvoltages. However, the developed solution leads to conflicting objectives since there is a strong coupling between VR and VUM.

To address current overload, congestion management (CM) techniques are employed, typically combined with VR methods. More specifically, the authors in [22] propose a generic, optimal management framework operating in various time frames. A consensus algorithm is proposed in [23] aiming to control the active power of DBESSs, while in [24], the well-established alternating direction method of multipliers is used to optimally coordinate the response of DRESs and DBESSs. Finally, in [25], the optimal coordination of DBESSs is achieved by solving the corresponding optimization problem with the aid of a multi-agent system. These methods have been developed assuming balanced grids constituting their application to unbalanced cases highly questionable.

Based on the above analysis, it can be deduced that literature lacks of a unified approach for unbalanced LV distribution grids that combines VR, VUM, and CM techniques. A potential solution is to mathematically formulate this problem and apply optimization techniques. A preliminary analysis is presented in [26] where DRESs are optimally engaged to control the phase-to-neutral voltages using generation and consumption forecasts. However, this approach is characterized by increased computational complexity and volatility to forecast errors limiting its applicability under real field conditions. This paper aims to fill this gap by developing a unified control strategy for unbalanced LV distribution grids, consisting of three new algorithms concerning VR, VUM, and CM. The unified strategy uses DRESs and DBESSs as the main control units by exploiting their reactive and active power capability. The core of the proposed algorithms is their implementation in the symmetrical components domain. In particular, the VR and CM methods regulate the positive sequence voltages and currents, respectively, while the VUM algorithm aims to reduce the zero- and the negative-sequence voltages. In such a manner the proposed VR becomes also compliant with the requirements posed by the IEEE 1547 Standard [17]. The performance of the proposed control strategy is assessed by conducting time-domain and quasi-static simulations. In the former case, the performance of the adopted VR and CM algorithms is evaluated considering the time delay of the communication infrastructure. In the latter case, the proposed VUM and VR methods are compared with several control schemes of the relevant literature. In this context, the strengths of the proposed unified strategy are summarized in the following:

- *Decoupled control algorithms.* Unlike the most relevant control schemes, the proposed VUM, VR and CM algorithms are decoupled, removing this way any interference among them and subsequently facilitating their accurate and efficient handling.
- *Low-complexity, measurement-based VR and CM algorithms*. Control actions are locally determined by each DRES/DBESS combining local measurements and information received from a central controller (CC) via communication infrastructure. In addition, the proposed algorithms fully exploit the reactive power capability of DRES/DBESS converters to reduce the use of active power either curtailed at DRESs or stored at DBESSs.
- *Introduction of the damping susceptance*. Contrary to the damping conductance concept adopted in [19]–[21] that utilizes the active power as the main means for VUM, a damping susceptance is introduced within the proposed VUM method allowing the exploitation and control of the reactive power.
- *Improved DBESSs utilization*. The use of the active power of DBESSs is treated as the last resort in the proposed control strategy, reducing their usage and increasing the lifetime expectancy. Furthermore, a day-ahead planning algorithm is proposed to ensure the effective participation of DBESSs in the VR and CM of the next day.
- *Reduced network losses*. The proposed VR algorithm leads to reduced network losses against decentralized and distributed, measurement-based control schemes presented in the literature.

II. Proposed Unified Control Strategy

A. Overview

The architecture of the proposed methodology is presented in Fig. 1. It consists of two distinct implementation layers listed below:

- *The local controller (LC) layer*. This layer corresponds to the design of a LC that can be integrated in grid-interfaced converters of DRESs/DBESSs. Scope of the LC is to adjust the converter output power based only on the measurements acquired at the point of interconnection (POI) with the grid in order to address potential voltage violations, unbalances, and current overloads.
- *The CC layer*. In this layer, a CC is employed to coordinate the control actions taken by the LCs. The aim of the coordination procedure is twofold: (a) to avoid possible interference caused by the simultaneous triggering of LCs and (b) to identify LCs that should contribute towards a violation event.

A conceptual representation of the proposed unified strategy is depicted in Fig. 2 and comprises three individual control blocks referred to the VR, CM and VUM. Each block is employed to tackle a specific issue by executing appropriate algorithms. Considering VR and CM, the LC of the participating DRESs/DBESSs exchanges information with CC at regular intervals. In case a voltage violation or a current overload issue is detected, the CC prioritizes the response of DRESs/DBESSs by sending triggering signals (TSs) to the corresponding LCs to adjust their converter output power. On the other hand, the voltage unbalances are mitigated in a decentralized manner. In particular, the VUM control is always activated at the LC and the converter output currents are estimated according to the proposed VUM method.

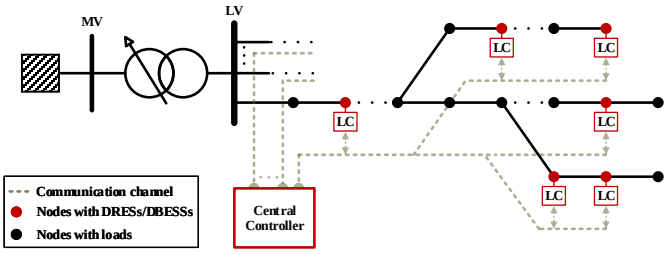

Fig. 1. Control architecture of the proposed method.

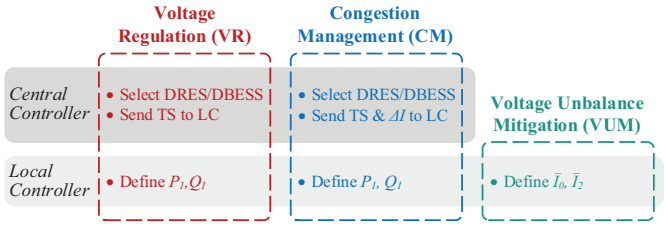

Fig. 2. Conceptual representation of the proposed unified control strategy.

The strategy layers and the individual control algorithms are discussed in detail in the following subsections.

B. LC Design Fundaments

The distinct feature of the proposed control strategy is the implementation of the LC in the symmetrical components domain. To this end, the symmetrical components of the POI voltages are calculated from the corresponding phase-to-neutral voltages as follows:

$$\begin{bmatrix}\bar{V}_0\\ \bar{V}_1\\ \bar{V}_2\end{bmatrix} = \begin{bmatrix}1 & 1 & 1\\ 1 & \bar{\alpha}^2 & \bar{\alpha}\\ 1 & \bar{\alpha} & \bar{\alpha}^2\end{bmatrix}^{-1} \begin{bmatrix}\bar{V}_a\\ \bar{V}_b\\ \bar{V}_c\end{bmatrix} = \mathbf{T}^{-1} \begin{bmatrix}\bar{V}_a\\ \bar{V}_b\\ \bar{V}_c\end{bmatrix} \quad (1)$$

where $\bar{V}_x$ denotes the complex phase-to-neutral voltage of phase $x = \{a, b, c\}$ and $\mathbf{T}$ is the transformation matrix from the symmetrical components to the unbalanced three-phase system. Furthermore, $\bar{\alpha} = e^{j\frac{2\pi}{3}}$ is the phasor rotation operator; $\bar{V}_y$ stands for the complex voltage of the symmetrical component $y = \{0, 1, 2\}$. The symmetrical components of the reference output currents of the DRESs/DBESSs are calculated according to

$$\begin{bmatrix}\bar{I}_0\\ \bar{I}_1\\ \bar{I}_2\end{bmatrix} = \underbrace{\begin{bmatrix}\underbrace{G_0 + jB_0}_{\bar{Y}_0} & 0 & 0\\ 0 & \underbrace{G_1 + jB_1}_{\bar{Y}_1} & 0\\ 0 & 0 & \underbrace{G_2 + jB_2}_{\bar{Y}_2}\end{bmatrix}}_{\mathbf{Y}} \begin{bmatrix}\bar{V}_0\\ \bar{V}_1\\ \bar{V}_2\end{bmatrix}. \quad (2)$$

Here, the admittance matrix $\mathbf{Y}$ consists of only diagonal, independent elements, i.e., $\bar{Y}_0$, $\bar{Y}_1$, and $\bar{Y}_2$, allowing the individual handling of each symmetrical component at the DRES/DBESS level. For example, the zero-sequence output current of the converter is determined based only on the zero-sequence POI voltage. Additionally, considering distribution lines it is important to stress out that they are characterized by a symmetric impedance matrix with almost equal off-diagonal elements [27]. This way, the corresponding symmetrical components admittance matrix can be also assumed diagonal, since the resulting off-diagonal terms are small compared to the diagonal ones. Consequently, the symmetrical components can be considered fully decoupled and can be independently controlled at the grid level. The values of $\bar{Y}_0$ and $\bar{Y}_2$ refer to the proposed VUM technique, while $\bar{Y}_1$ is calculated as follows:

$$\bar{Y}_1 = \frac{\bar{S}_1^*}{3|\bar{V}_1|^2} \quad (3)$$

where $\bar{S}_1$ is the positive-sequence complex power determined according to the proposed VR method. It is evident that VR is fully decoupled from VUM by adopting this approach. The final injected DRESs/DBESSs currents in the unbalance three-phase system are calculated by using (4).

$$\mathbf{I_{abc}} = \mathbf{TYT}^{-1}\mathbf{V_{abc}} \quad (4)$$

$\mathbf{I_{abc}}$ and $\mathbf{V_{abc}}$ stand for the phase current and the phase-to-neutral voltage vectors, respectively.

C. Voltage Unbalance Mitigation

According to the proposed VUM control strategy, $\bar{Y}_0$ and $\bar{Y}_2$ in (2) are treated as pure imaginary parameters introducing the damping susceptance concept. As a result, DRESs/DBESSs use only zero- and negative-sequence reactive currents ($\bar{I}_0$ and $\bar{I}_2$ - See also Fig. 2), and subsequently reactive power, to mitigate voltage unbalances. The contribution of each unit to the VUM strongly depends on the damping susceptance. High damping susceptance increases the output currents, which, in turn, leads to higher compensation of voltage unbalances. The reason behind the use of the reactive power is twofold: (a) reduce DBESS utilization by avoiding the use of active power and (b) ensure that VUM is at disposal in cases the active power of DBESSs/DRESs is not available, e.g., empty DBESSs, DRESs with zero production, etc. Following this approach, VUM can be always activated ensuring the effective reduction of network asymmetries.

D. Voltage Regulation

Another key feature of the proposed VR strategy is the control of the positive-sequence network voltages, being in line with the IEEE 1547 Standard [17]. This is attained by controlling only the positive-sequence complex output power of DRESs/DBESSs following a low-complexity, measurement-based procedure. Considering overvoltage mitigation, this procedure is presented in Fig. 3 by means of a flowchart; a similar rationale is followed for undervoltage mitigation that usually occurs during the night where electricity production from DRESs (PVs) is not available. It is worth mentioning that the control actions adopted by this procedure are performed by the LCs combining local measurements and information received from the CC. Towards this objective, a two-way

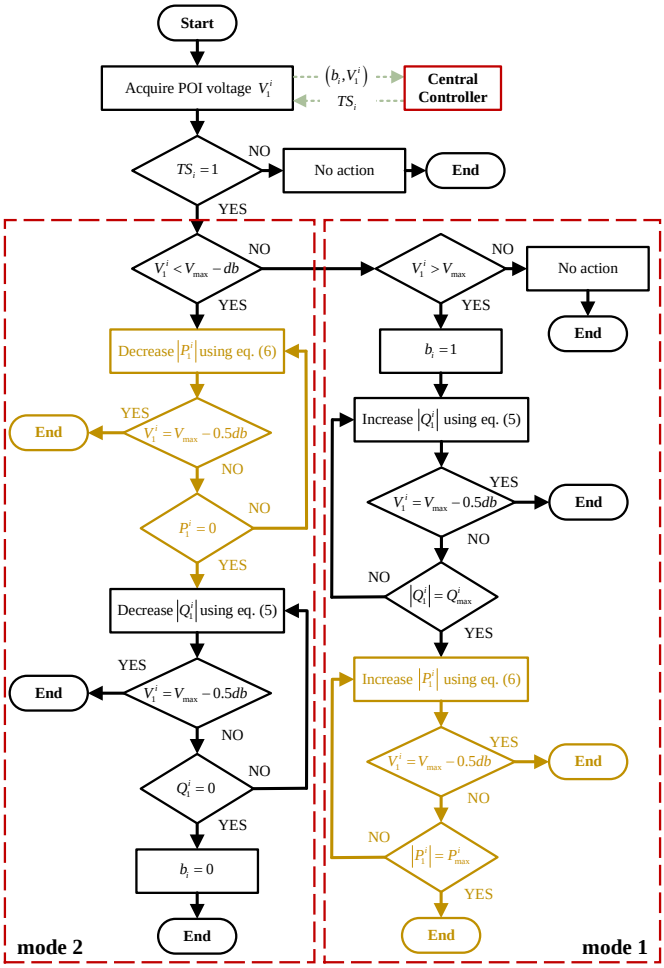

Fig. 3. Operation scheme of the DRES/DBESS located at node i for overvoltage mitigation. The process denoted with yellow color is absent in case of DRES.

communication channel is established between LCs and CC. The data sent by LCs are the positive-sequence POI voltage and a binary variable indicating whether the DRES/DBESS exchanges zero (0) or non-zero (1) power with the grid to control the POI voltage. The CC sends individualized TSs to each LC. An analytical description of this procedure is provided below.

Assuming only a DBESS unit located at node i, the LC constantly monitors the positive-sequence POI voltage (V_1^i) which, along with the binary variable (b_i), is transmitted to the CC on a regular basis, i.e., every few hundreds of milliseconds or several seconds. The proposed VR control strategy consists of two operating modes, namely mode 1 and mode 2. These are separated by a small deadband (db), where no actions occur to avoid oscillations and recurrent switching between these modes. The deadband is determined by the accuracy of the measurement devices, without, however, affecting the performance of the proposed VR control strategy.

In particular, mode 1 deals with overvoltage mitigation giving priority to the use of reactive power against active power to reduce DBESS utilization. This mode is triggered when both conditions are met, i.e., (a) TS_i received by the CC is equal to 1 and (b) V_1^i exceeds the maximum permissible voltage limit ($V_{\max}$). As long as TS_i is equal to 1, a proportional-integral (PI) controller is employed in (5) to determine the reactive power of DBESS (Q_1^i - See also Fig. 2) by eliminating the error between V_1^i and the reference voltage $V_{\text{ref}} = V_{\max} - 0.5db$.

$$Q_1^i = -\left(k_p + \frac{k_i}{s}\right)\left(V_1^i - V_{\text{ref}}\right) \tag{5}$$

Here, k_p and k_i are the proportional and the integral gains of the PI controller, respectively. Note that a positive Q_1^i value refers to overexcitation, i.e., the DRES/DBESS injects reactive power to the grid, while a negative Q_1^i value denotes reactive power absorption. Thus, the absolute value of Q_1^i is employed in the flowchart of Fig. 3 to indicate that the amount of the absorbed reactive power is increased to reduce the voltage. A similar rationale is adopted for the active power of the DBESS (P_1^i - See also Fig. 2). This process continues till either the POI voltage is regulated or the maximum available reactive power ($Q_{\max}^i$), which is calculated according to the analysis presented in [28], is reached. In the latter case, the DBESS starts the charging process by absorbing P_1^i using a PI controller according to (6). Provided that TS_i is equal to 1, the active power of DBESS increases till the voltage is finally regulated or the maximum active power ($P_{\max}^i$) is reached.

$$P_1^i = -\left(k_p + \frac{k_i}{s}\right)\left(V_1^i - V_{\text{ref}}\right) \tag{6}$$

After mode 1 is completed, DBESS switches to constant power operation. Therefore, the possible varying network operating conditions may result to unnecessary power absorption of DBESS. To avoid such cases, mode 2 is introduced. Specifically, it is activated when TS_i is equal to 1 and the POI voltage is reduced below $V_{\max} - db$. First, the active power of DBESS is reduced till the POI voltage is regulated or the active power becomes zero. In the latter case, the process moves to the reduction of the reactive power till zero unless the voltage is regulated. Note that, in case of DRESs units located at node i, the proposed VR control strategy is limited to using only the reactive power to avoid the curtailment of green energy.

The operation scheme of the CC for overvoltage mitigation is depicted in the flowchart Fig. 4. Initially, the positive-sequence POI voltages and the corresponding binary variables are acquired from the LCs. Afterward, the CC determines the LC node with the maximum POI voltage. In case the POI voltage exceeds $V_{\max}$, the VR of the corresponding LC is activated by sending a TS equal to 1. On the other hand, a maximum POI voltage less than $V_{\max} - 0.5db$ indicates that mode 2 should be activated by properly reducing the locally absorbed power. The activation sequence follows the network voltage profiles from the LC node with the minimum to the maximum voltage. Note that by adopting a similar rationale, the operation scheme of the CC for undervoltage mitigation can be derived.

In light of the above analysis, it can be realized that the proposed VR control strategy is an event-triggered method, i.e., it is activated only when the voltage limits are violated. Although this approach leads to a reduced use of active and reactive

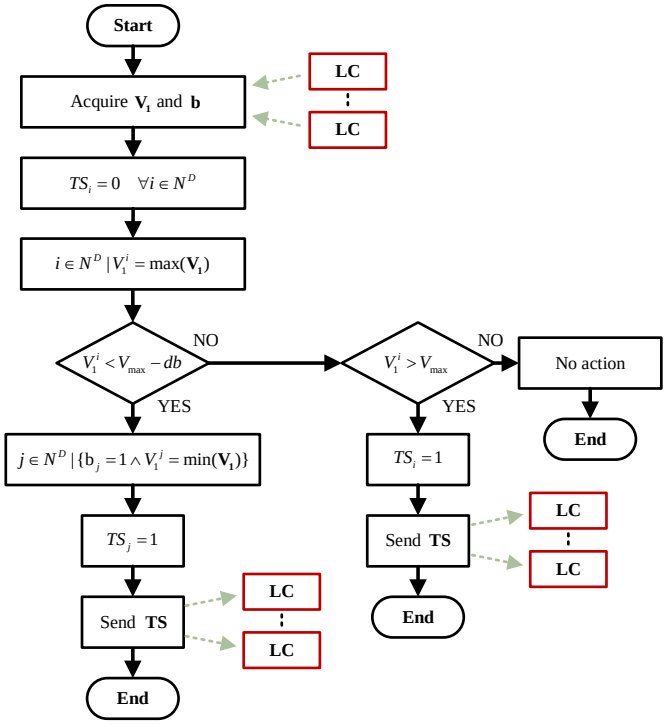

Fig. 4. Operation scheme of the CC for overvoltage mitigation. N^{D} denotes the set of network nodes where DRESs/DBESSs are installed.

power for VR, it cannot ensure the availability of DBESSs to provide active power support since their storage capability is limited due to their sizing constraints. To overcome this issue, a day-ahead planning algorithm is proposed aiming to ensure that a sufficient amount of energy can be provided or stored by the DBESSs in the next day to ensure their effective participation in the VR; this process is undertaken by the CC. In particular, considering overvoltage mitigation, the proposed algorithm works as follows. Forecasted day-ahead generation and consumption profiles are used in order to perform quasi-static simulations employing the proposed VR method. By the conducted simulations, the required storage range (SR_i), i.e., the amount of energy that will be stored during VR process by the DBESS located at node i in the next day, is estimated. To mitigate possible miscalculations caused by the forecast errors a safety factor (sf) is assumed to calculate the final value of SR_i. Subsequently, under real-field conditions, considering the obtained results of the proposed day-ahead planning algorithm, a discharging process with constant power is applied to the DBESS connected to node i during no-generation periods to reach a storing capability equal to the corresponding $sf \cdot SR_i$. Note that, a similar process can be followed for the undervoltage mitigation.

E. Congestion Management

The conceptual design of the proposed CM scheme is presented in Fig. 5. Scope of the proposed method is to tackle current overloads considering minimum interference with the proposed VR and VUM methods. Towards this objective, the proposed CM scheme is implemented in the positive-sequence, i.e., positive-sequence currents flowing through the lines are

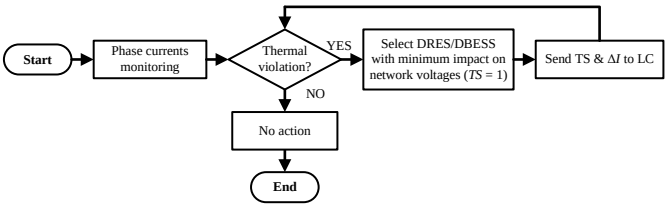

Fig. 5. Operation scheme of the CC for congestion management.

controlled by modifying the positive-sequence active and reactive power of DRESs/DBESSs, thus removing any interference with the VUM. Furthermore, a new process is proposed to select the most suitable DRESs/DBESSs that will participate in the proposed CM in terms of minimizing their impact on the VR. The CC is employed to coordinate the response of the LCs in the proposed CM scheme. More specifically, the CC constantly monitors the phase currents flowing through the medium-/low-voltage (MV/LV) transformer and the lines close to or directly connected to the LV busbar, constituting the best candidates for current overload due to the radial configuration of LV distribution grids [23]. The operation of the proposed CM scheme is analytically described below.

Assuming a thermal violation of phase x of the branch connecting node i with node j, the CC initially estimates the excess amount of current ΔI which is equal to $|\bar{I}_x^{ij}| - I_{\max}^{ij}$. Afterward, in order to minimize the interference between CM and VR, the CC selects the DRES/DBESS connected to the node with the lowest impact on network voltages to participate in the proposed CM scheme. This impact is quantified by using the sensitivity matrix as follows:

$$\begin{bmatrix} \Delta\boldsymbol{\theta_1} \\ \Delta|\bar{\mathbf{V}}_\mathbf{1}| \end{bmatrix} = \mathbf{J_1^{-1}} \begin{bmatrix} \Delta\mathbf{P_1} \\ \Delta\mathbf{Q_1} \end{bmatrix} = \begin{bmatrix} \mathbf{k} & \mathbf{l} \\ \mathbf{m} & \mathbf{n} \end{bmatrix} \begin{bmatrix} \Delta\mathbf{P_1} \\ \Delta\mathbf{Q_1} \end{bmatrix} \tag{7}$$

where $\mathbf{J_1^{-1}}$ is the inverse Jacobian matrix in the positive-sequence quantifying the voltage magnitude $\Delta|\bar{\mathbf{V}}_\mathbf{1}|$ and angle ($\Delta\boldsymbol{\theta_1}$) variations with respect to active ($\Delta\mathbf{P_1}$) and reactive power ($\Delta\mathbf{Q_1}$) fluctuations. Since both the active and reactive power are used as the main means of controlling the network currents, the sub-matrices $\mathbf{m}$ and $\mathbf{n}$ of (7) are of main importance, as they refer to the voltage variations against active and reactive power injections, respectively.

Following the identification of the DRES/DBESS, the CC sends a TS value equal to 1 as well as the calculated ΔI to the corresponding LC. Between active and reactive power, priority is given to the reactive power to reduce the DBESS utilization. A PI controller is used to determine the reactive power output by eliminating the error between the actual measured ΔI_m and the reference value (ΔI) similarly to (5). If the maximum reactive power is reached, the active power of DBESS is used to regulate the network currents. Subsequently, in case the maximum active power is reached, the process moves to the next DRES/DBESS with the lowest impact on network voltages. Note that, the new DRES/DBESS is selected by using (7). Apart from the new TS value (from 0 to 1), an updated value of ΔI (depended on the effectiveness of the previous DRES(s)/DBESS(s)) is forwarded by the CC to the

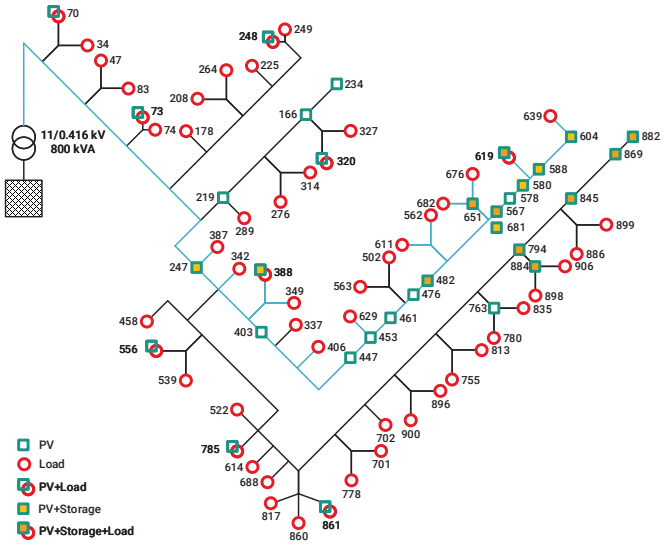

Fig. 6. Topology of the IEEE LV test feeder. The part of the grid denoted with blue color is considered in the time-domain simulations.

new DRES/DBESS. This procedure is repeated till the currents are finally regulated. In case of no congestion issues are observed, the reverse process of reducing the output power for DRESs/DBESSs is applied accordingly by adopting a similar approach.

III. Numerical Results

A. System Under Study

The performance of the unified control strategy is evaluated by conducting time-domain and quasi-static simulations on the unbalanced three-phase IEEE European LV test feeder depicted in Fig. 6. According to [29], the original version of the examined configuration refers to a passive network feeding 55 single-phase loads. To assess the proposed control strategy, the IEEE LV test feeder is modified by adding 32 PVs and 15 DBESSs, as shown in Fig. 6. The connection node and the installed capacity of PVs and DBESSs are presented in Tables I and II, respectively. The power factor (PF) of the single-phase loads is 0.95 lagging and the nominal PF of PVs and DBESSs is 0.85. The minimum ($SOC_{\min}$) and maximum ($SOC_{\max}$) state-of-charge of the DBESSs are 0.1 and 0.9, respectively; the charging/discharging efficiency is 0.95. Finally, the minimum ($V_{\min}$) and maximum ($V_{\max}$) permissible voltage limits are assumed equal to 0.9 and 1.1 pu.

B. Time-Domain Simulations

Time-domain simulations are conducted by using the PSIM software [30] to assess the performance of the proposed CM and VR methods. Since both methods are implemented in the positive-sequence, a balanced network is used considering only the positive-sequence components of the lines; loads and PVs are modelled using a three-phase, balanced configuration. Furthermore, to accelerate the execution time of the simulation process, a reduced version of the IEEE European LV test

TABLE I
PV Installed Capacity

Node	kWp
70, 166, 234, 247, 248, 388, 403, 447, 453, 482, 556, 567, 580, 588, 619, 651, 763, 785, 845, 861, 869, 884	7.5
73, 219, 320, 461, 476, 578, 604, 681, 794, 882	15

TABLE II
DBESSs Installed Capacity

Node	kWh	kW	Node	kWh	kW
247, 388, 482, 681, 845	10	5	869	15	7.5
567, 580, 588	22.5	7.5	882	25	12.5
794, 884	5	2.5	604	45	15
619, 651	30	7.5			

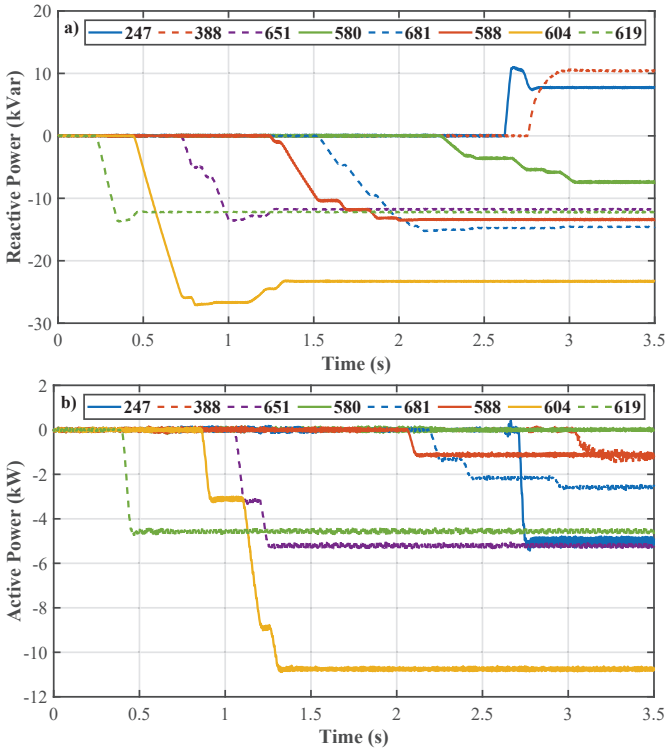

Fig. 7. Output power of PVs and DBESSs. (a) Aggregated reactive power of PVs and DBESSs and (b) active power of DBESSs.

feeder is assumed, as depicted in Fig. 6. Considering VR, the voltage deadband (db) is equal to 0.01 pu. The proposed VR and CM methods are assessed under the worst-case scenario in terms of reverse power flow. This occurs at 13:53 h where the injected power by the PVs is equal to their rated value. The absorbed power of the loads is determined by the corresponding profiles presented in [29]. The thermal limit of the lines of the backbone of the network is assumed equal to 255 A (originally in [29] no current limits are provided). Finally, the voltage at the slack bus is 1.0675 pu.

In addition, to include the ICT system in the simulations, a communication delay equal to 20 ms is assumed regarding the information exchanged between the CC and the LCs. Moreover, the measured current and the voltage sent by the

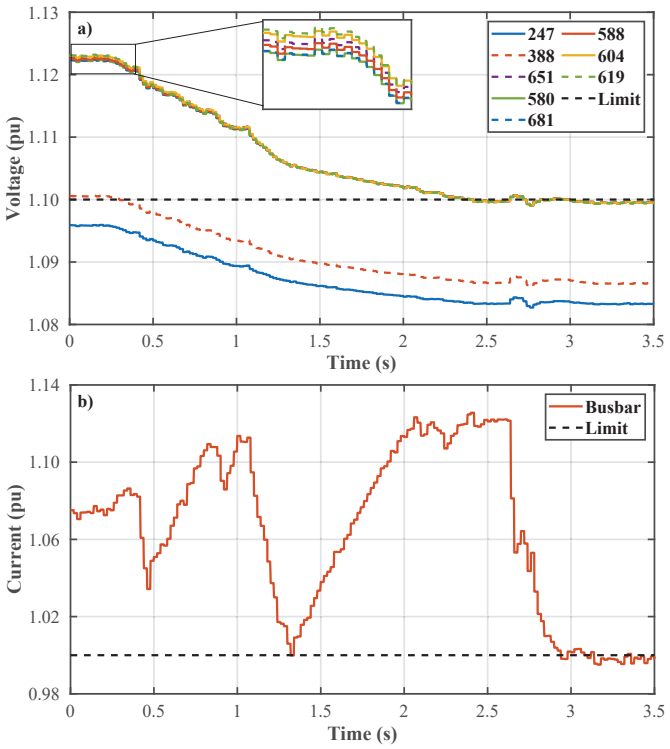

Fig. 8. Network operating condition. (a) RMS voltage and (b) RMS current magnitudes.

PVs are modeled as discrete signals updated every 20 ms. Relatively small rates have been selected to reduce the overall simulation time. Under real-field conditions, these values may increase, without affecting the performance of the proposed method.

The output power of the PVs and DBESSs participating in the proposed VR and CM methods is depicted in Fig. 7 and the network voltages and the current flowing at the sending-end of the backbone line, i.e., at the distribution substation LV busbar, are presented in Figs. 8a and 8b, respectively. Note that, the aggregated PV and DBESS reactive power at PV/DBESS nodes is depicted in Fig. 7a.

Initially, DBESSs remain idle and PVs operate with unity power factor leading to thermal and voltage violations, as verified in Fig. 8. The proposed VR method is activated at 0.2 s.

The CC changes the TS value sent to node 619, i.e., the node with the maximum network voltage (see Fig. 8a) from 0 to 1. After the delay of 20 ms, the LCs of both the PV and DBESS connected at node 619 receive the new TS value and start absorbing reactive power (mode 1) till the maximum limits are reached at 0.35 s. At this time instant, the TS value sent to node 619 remains equal to 1 since the maximum network voltage continues at this node (see Fig. 8a). As a result, the VR procedure moves to the use of the active power of DBESS (P_b) implementing the control logic analysed in Fig. 3. After a time period of 50 ms, i.e., at 0.4 s, the DBESS at node 619 starts absorbing active power. During this process, the reactive power of the DBESS (Q_b) is automatically adjusted as shown in Fig. 7a to satisfy the reactive power capability of the DBESS according to $Q_b = \sqrt{{S_b}^2 - {P_b}^2}$, where S_b is the nominal apparent power of the DBESS converter. Note that the 50 ms time period for the activation of the active power control of DBESS is selected to demonstrate the intermediate steps of the proposed VR method. Under real-field conditions, this time period can be zero to accelerate the convergence of the proposed VR method.

Shortly after the use of the DBESS active power, i.e., at 0.42 s, the location of the maximum network voltage changes from node 619 to node 604. Therefore, the CC changes the TS values sent to nodes 604 and 619 from 0 to 1 and from 1 to 0, respectively. After the delay of 20 ms, this information is received by the LCs at nodes 619 and 604. The former switches to a constant power operation while the latter initiates the reactive power absorption process as described in Fig. 3. The VR process continues with the remaining PVs and DBESSs following the control logic described above till the network voltages are finally regulated at 2.4 s, as shown in Fig. 8a.

According to Fig. 8b, it can be realized that the thermal violation persists since the proposed VR method leads to a further increase of the current at the backbone line. This is mainly caused by the use of the reactive power. To tackle this violation, the proposed CM method is activated at 2.6 s. As a first step, the CC employs sensitivity theory to identify the PV/DBESS node with the lowest impact on the network voltages, namely node 247. Afterward, the CC changes the TS value sent to the LCs of both the PV and DBESS connected at node 247 from 0 to 1. Moreover, the CC sends the calculated data of $\Delta I = 0.12$ pu. After a communication delay of 20 ms, i.e., at 2.62 s, the PV and the DBESS start injecting reactive power to the grid to compensate locally the reactive power flow till the maximum limit is reached at 2.65 s. Following a time period of 50 ms, i.e., at 2.7 s, the DBESS at node 247 starts increasing the absorbed active power up to the maximum limit. Note that, the specific limit is reached at 2.74 s. The proposed CM continues with the next PV/DBESS node, i.e., node 388 (by means of sensitivity analysis), till the line current is finally regulated at 3.1 s. It is worth mentioning that the impact of the proposed CM method on the network voltages is practically negligible, as shown in Fig. 8a.

Based on the above analysis, it can be deduced that the proposed CM and VR methods can effectively mitigate voltage and thermal violations by keeping their interference to a minimum level. Note that the corresponding remarks, regarding the interference between VR and CM as well as the deactivation sequence of PVs/DBESSs participated in the proposed CM scheme, are also derived for the second operating mode concerning the reduction of the PVs/DBESSs output power.

C. Long-term Evaluation

Quasi-static simulations of 1-min resolution are conducted to evaluate the long-term performance of the proposed VR and VUM control strategies. The simulation period is two days, i.e., a sunny day followed by a cloudy day. The daily load and generation profiles are derived from [29] and [31], respectively. To evaluate the day-ahead planning algorithm, forecast errors are assumed for the second day of the analysis. Specifically,

the load profiles are arbitrary located at network load nodes considering the random behaviour of LV consumers. Note that the peak load demand of each node is maintained equal to the original one [29]. Regarding the generation profiles, a forecast error equal to 5% is also assumed. The proposed approach is compared against well-established control schemes (CSs) proposed in literature considering the following scenarios:

- Proposed VR (PVR). In this scenario, only the proposed VR method is employed.
- Proposed VR with VUM (PVRUM). The proposed VR method is combined with the proposed VUM control algorithm assuming $\bar{Y}_0 = \bar{Y}_2 = j4$ S.
- Control scheme 1 (CS1) is dealing with a consensus algorithm for VR using only the positive-sequence active power of DBESSs [5].
- Control scheme 2 (CS2). In this scenario, the decentralized, droop-based $Q(V) - P(V)$ method proposed in [9] is adopted to control the output power of both PVs and DBESSs. The settings of the $Q(V)$ and $P(V)$ droop curves are assumed equal to $V_i^{aQ} = 1.08$ pu and $V_i^{tP} = 1.09$ pu. Note that the $P(V)$ droop-curve is only applied to control the output active power of DBESSs.
- Control scheme 3 (CS3) is a phase-based implementation of the consensus algorithm proposed in [13] for VR using only the active power of DBESSs.
- Control scheme 4 (CS4). This is a droop-based $P(V)$ solution proposed in [19] with deactivated VUM, i.e., $\bar{Y}_0 = \bar{Y}_2 = 0$ S.
- Control scheme 5 (CS5). This is an alternative version of the method presented in [19] with activated VUM, i.e., $\bar{Y}_0 = \bar{Y}_2 = j4$ S. Note that in both versions, the voltage thresholds V_{cdb} and V_{vpb} are equal to 1.07 and 1.09 pu, respectively.

Furthermore, to ensure a common comparative basis, the proposed day-ahead planning algorithm is integrated to all CSs assuming a sf equal to 0.05.

The two-day profile of the positive-sequence voltage at node 619 (the maximum voltage levels), is depicted in Fig. 9. Additionally, the overall reactive energy used by the PVs (E^Q_{PVs}) and DBESSs (E^Q_{DBESSs}) is summarized in Table III. The impact of each CS on the voltage asymmetries is evaluated by means of cumulative distribution function (CDF) plots presented in Figs. 10a and 10b; the CDF plots correspond to the zero- (VUF0) and the negative-sequence (VUF2) voltage unbalance factors [21], respectively. Moreover, the total energy absorbed by DBESSs is shown in Table IV. Finally, the total network losses and the utilization of DBESSs are analysed in Figs. 11a and 11b.

According to Fig. 9 and Table III, it can be realized that active power-based solutions, i.e., CS1, CS3-CS5, cannot tackle overvoltages due to the limited storage capacity of DBESSs. On the other hand, by using the reactive power as an additional voltage regulation means, overvoltages are effectively mitigated considering PVR, PVRUM, and CS2. Nevertheless, CS2 leads to the narrowest voltage profile. This is attributed to the use of the droop curve which activates the reactive power absorption process for voltages lower than $V_{\max}$ and consequently to increased use of reactive energy, as

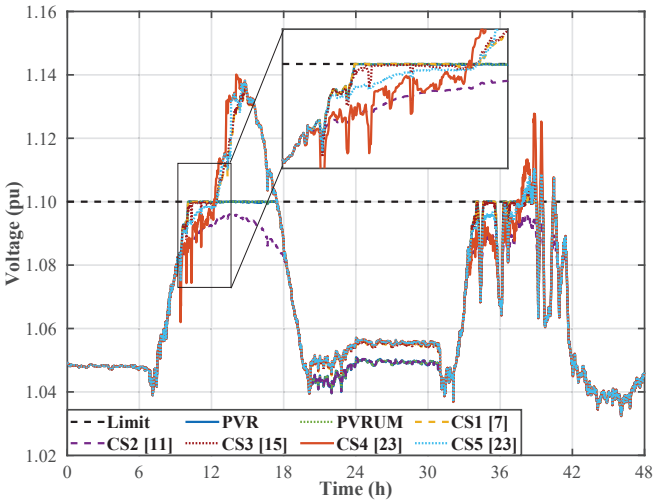

Fig. 9. Profile of the positive-sequence voltage at node 619.

TABLE III
OVERALL REACTIVE ENERGY ABSORBED BY PVS AND DBESSS

Examined CSs	E^Q_{PVs} (kVarh)	E^Q_{DBESSs} (kVarh)	Voltage Within Limits
PVR	621.35	751.64	YES
PVRUM	625.32	755.51	YES
CS1 [7]	-	-	NO
CS2 [11]	1209.61	1136.45	YES
CS3 [15]	-	-	NO
CS4 [23]	-	-	NO
CS5 [23]	-	-	NO

shown in Table III. On the contrary, both PVR and PVRUM are event-triggered methods, i.e., they are activated only when the voltage exceeds $V_{\max}$. As a result, the total absorbed reactive energy is lower by 41.5% and 41.1%, respectively, compared to CS2. Similar observations can be made regarding the network energy losses which are lower by 25.7 % and 24.4 % against CS2, as shown in Fig. 11a. Note that no direct comparison can be done between CS1, CS3-CS5 and the examined control strategies in terms of network losses, since the network voltages are not maintained within the permissible limits (see Fig. 9).

Considering CS4 and CS5, it is evident that the activation of the VUM affects the profile of the positive-sequence voltage, as verified in Fig. 9; thus a strong coupling between VR and VUM is indicated. On the contrary, both implementations of the proposed method, i.e., PVR and PVRUM, lead to identical positive-sequence voltage profiles, revealing the complete decoupling between VR and VUM.

Regarding voltage asymmetries, it can be observed that both VUF0 and VUF2 acquire the lowest values when PVRUM is employed. It should be also mentioned that although for CS3 and CS5 the network asymmetry has been improved, the corresponding results cannot be evaluated, since both CSs fail to tackle network overvoltages. Moreover, it can be seen that when PVR is examined, both VUF0 and VUF2 are similar to those obtained in CS2. This reveals that the proposed VR

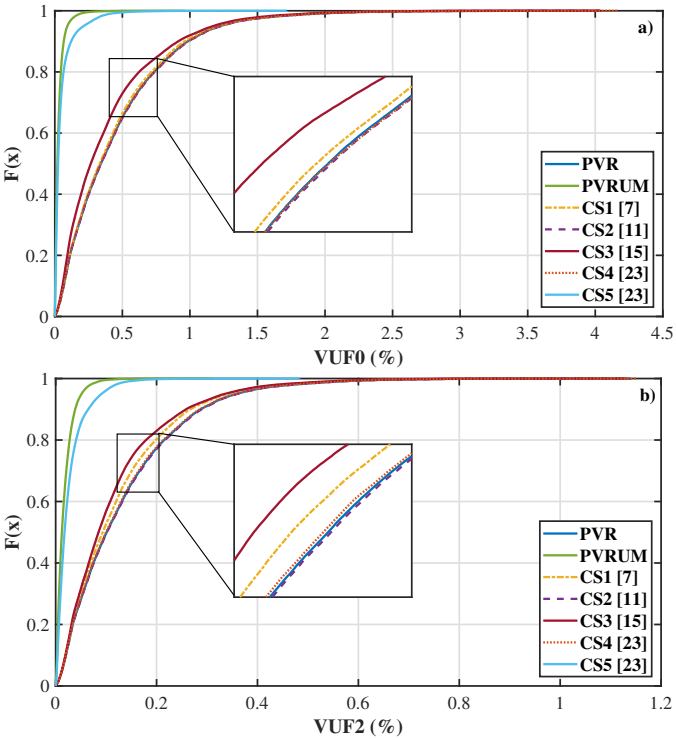

Fig. 10. Cumulative distribution function. (a) VUF0 and (b) VUF2.

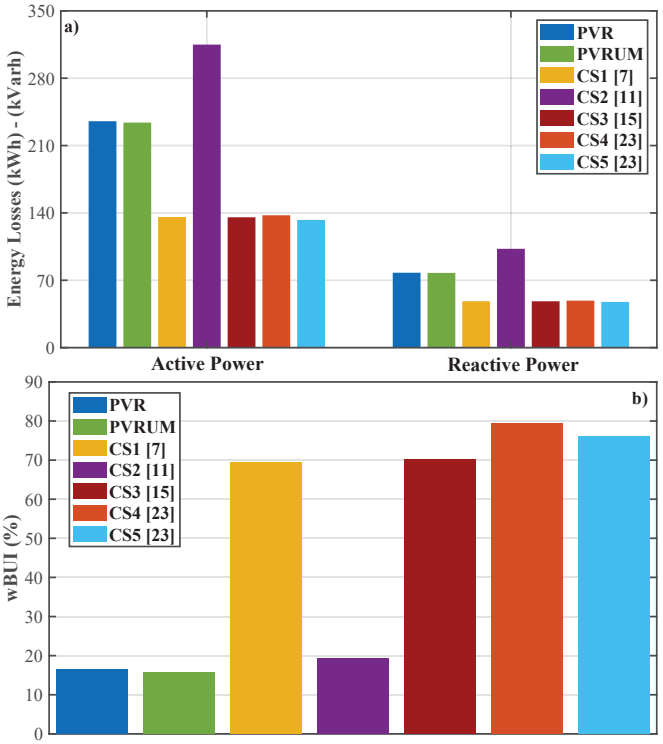

Fig. 11. Network and DBESS evaluation. (a) Total network energy losses and (b) weighted DBESS utilization index (wBUI).

TABLE IV
TOTAL ENERGY ABSORBED BY DBESSS

Examined CSs	Energy (kWh)	Examined CSs	Energy (kWh)
PVR	173.55	CS3 [15]	378.02
PVRUM	169.68	CS4 [23]	402.25
CS1 [7]	375.26	CS5 [23]	393.61
CS2 [11]	196.45		

algorithm does not affect the zero- and negative-sequence network voltages.

In terms of DBESSs utilization, both PVR and PVRUM present the lowest energy absorption as shown in Table IV. This is also verified in Fig. 11b, where the DBESSs utilization is quantified adopting the weighted DBESSs utilization index (wBUI) calculated as follows:

$$wBUI = \frac{\sum\limits_{i \in N^{\mathrm{D}}} B_i \cdot E_n}{d \cdot \sum\limits_{i \in N^{\mathrm{D}}} E_i^r} \cdot 100\% \tag{8}$$

where E_i and E_i^r are the total absorbed energy and the installed capacity of the DBESS connected to node i, respectively, d is the examined period in days, and B_i is a quantification index introduced in [32].

Results reveal that PVRUM leads to reduced usage of DBESSs up to almost 63% compared to the examined distributed and decentralized CSs. This implies that the proposed method results in decelerated cyclic aging of DBESSs and subsequently in calendar life expansion. This is also reflected in Fig. 9, where different voltage profiles are observed among the examined CSs during the DBESS discharging operation activated between 20:25 h - 07:00 h.

IV. CONCLUSION

In this paper, a unified approach for unbalanced LV distribution grids is proposed combining new VR, VUM, and CM algorithms. The developed algorithms are characterized by low-complexity, reduced monitoring needs, and limited exchange of information, facilitating their integration to the real distribution grids. The distinct feature of the proposed approach is that the adopted algorithms are decoupled allowing the individual handling of VR, VUM, and CM issues. By performing time-domain and time-series simulation, it is concluded that the proposed approach outperforms existing solutions proposed in the literature, in terms of reduced network losses, improved DBESS utilization and ability to concurrently address VR, VUM, and CM issues.

REFERENCES

[1] X. Xing, J. Lin, C. Wan, and Y. Song, "Model predictive control of lpc-looped active distribution network with high penetration of distributed generation," *IEEE Trans. Sustain. Energy*, vol. 8, no. 3, pp. 1051–1063, 2017.

[2] *Establishing the framework for achieving climate neutrality and amending regulation (EU) 2018/1999*, Proposal for a regulation, European Parliament and Council, Brussels, Belgium, 2020, pp. 1–46.

[3] R. A. Walling, R. Saint, R. C. Dugan, J. Burke, and L. A. Kojovic, "Summary of distributed resources impact on power delivery systems," *IEEE Trans. Power Del.*, vol. 23, no. 3, pp. 1636–1644, 2008.

[4] K. E. Antoniadou-Plytaria, I. N. Kouveliotis-Lysikatos, P. S. Georgilakis, and N. D. Hatziargyriou, "Distributed and decentralized voltage control of smart distribution networks: Models, methods, and future research," *IEEE Trans. Smart Grid*, vol. 8, no. 6, pp. 2999–3008, 2017.

[5] Y. Wang, K. T. Tan, X. Y. Peng, and P. L. So, "Coordinated control of distributed energy-storage systems for voltage regulation in distribution networks," *IEEE Trans. Power Del.*, vol. 31, no. 3, pp. 1132–1141, 2016.

[6] Z. Tang, D. J. Hill, and T. Liu, "Distributed coordinated reactive power control for voltage regulation in distribution networks," *IEEE Trans. Smart Grid*, vol. 12, no. 1, pp. 312–323, 2021.

[7] S. M. N. R. Abadi, A. Attarha, P. M. Scott, and S. Thiebaux, "Affinely adjustable robust Volt/Var control for distribution systems with high PV penetration," *IEEE Trans. Power Syst.*, article in press.

[8] M. Kabir, Y. Mishra, G. Ledwich, Z. Xu, and R. Bansal, "Improving voltage profile of residential distribution systems using rooftop pvs and battery energy storage systems," *Applied Energy*, vol. 134, pp. 290–300, 2014.

[9] T. T. Mai, A. N. M. Haque, P. P. Vergara, P. H. Nguyen, and G. Pemen, "Adaptive coordination of sequential droop control for PV inverters to mitigate voltage rise in PV-rich LV distribution networks," *Electr. Power Syst. Res.*, vol. 192, p. 106931, 2021.

[10] R. Zafar, J. Ravishankar, J. E. Fletcher, and H. R. Pota, "Multi-timescale model predictive control of battery energy storage system using conic relaxation in smart distribution grids," *IEEE Trans. Power Syst.*, vol. 33, no. 6, pp. 7152–7161, 2018.

[11] H. Xu, A. D. Domínguez-García, V. V. Veeravalli, and P. W. Sauer, "Data-driven voltage regulation in radial power distribution systems," *IEEE Trans. Power Syst.*, vol. 35, no. 3, pp. 2133–2143, 2020.

[12] S. Hashemi and J. Østergaard, "Efficient control of energy storage for increasing the PV hosting capacity of LV grids," *IEEE Trans. Smart Grid*, vol. 9, no. 3, pp. 2295–2303, 2018.

[13] M. Zeraati, M. E. Hamedani Golshan, and J. M. Guerrero, "A consensus-based cooperative control of PEV battery and PV active power curtailment for voltage regulation in distribution networks," *IEEE Trans. Smart Grid*, vol. 10, no. 1, pp. 670–680, 2019.

[14] J. Li, C. Liu, M. E. Khodayar, M. H. Wang, Z. Xu, B. Zhou, and C. Li, "Distributed online var control for unbalanced distribution networks with photovoltaic generation," *IEEE Trans. Smart Grid*, vol. 11, no. 6, pp. 4760–4772, 2020.

[15] X. Zhou, Z. Liu, C. Zhao, and L. Chen, "Accelerated voltage regulation in multi-phase distribution networks based on hierarchical distributed algorithm," *IEEE Trans. Power Syst.*, vol. 35, no. 3, pp. 2047–2058, 2020.

[16] M. S. S. Abad and J. Ma, "Photovoltaic hosting capacity sensitivity to active distribution network management," *IEEE Trans. Power Syst.*, vol. 36, no. 1, pp. 107–117, 2021.

[17] "IEEE standard for interconnection and interoperability of distributed energy resources with associated electric power systems interfaces," *IEEE Std 1547-2018 (Revision of IEEE Std 1547-2003)*, pp. 1–138, 2018.

[18] M. Yao, I. A. Hiskens, and J. L. Mathieu, "Mitigating voltage unbalance using distributed solar photovoltaic inverters," *IEEE Trans. Power Syst.*, article in press.

[19] D. V. Bozalakov, T. L. Vandoorn, B. Meersman, G. K. Papagiannis, A. I. Chrysochos, and L. Vandevelde, "Damping-based droop control strategy allowing an increased penetration of renewable energy resources in low-voltage grids," *IEEE Trans. Power Del.*, vol. 31, no. 4, pp. 1447–1455, 2016.

[20] D. Bozalakov, J. Laveyne, J. Desmet, and L. Vandevelde, "Overvoltage and voltage unbalance mitigation in areas with high penetration of renewable energy resources by using the modified three-phase damping control strategy," *Electr. Power Syst. Res.*, vol. 168, pp. 283–294, 2019.

[21] E. O. Kontis, G. C. Kryonidis, A. I. Nousdilis, K.-N. D. Malamaki, and G. K. Papagiannis, "A two-layer control strategy for voltage regulation of active unbalanced LV distribution networks," *Int. J. Electr. Power Energy Syst.*, vol. 111, pp. 216–230, 2019.

[22] A. Kulmala, M. Alonso, S. Repo, H. Amaris, A. Moreno, J. Mehmedalic, and Z. Al-Jassim, "Hierarchical and distributed control concept for distribution network congestion management," *IET Gener., Transm. & Distrib.*, vol. 11, no. 3, pp. 665–675, 2017.

[23] G. Mokhtari, G. Nourbakhsh, and A. Ghosh, "Smart coordination of energy storage units (ESUs) for voltage and loading management in distribution networks," *IEEE Trans. Power Syst.*, vol. 28, no. 4, pp. 4812–4820, 2013.

[24] C. Feng, Z. Li, M. Shahidehpour, F. Wen, W. Liu, and X. Wang, "Decentralized short-term voltage control in active power distribution systems," *IEEE Trans. Smart Grid*, vol. 9, no. 5, pp. 4566–4576, 2018.

[25] M. Bahramipanah, D. Torregrossa, R. Cherkaoui, and M. Paolone, "A decentralized adaptive model-based real-time control for active distribution networks using battery energy storage systems," *IEEE Trans. Smart Grid*, vol. 9, no. 4, pp. 3406–3418, 2018.

[26] A. S. Zamzam, N. D. Sidiropoulos, and E. Dall'Anese, "Beyond relaxation and Newton–Raphson: Solving AC OPF for multi-phase systems with renewables," *IEEE Trans. Smart Grid*, vol. 9, no. 5, pp. 3966–3975, 2018.

[27] K. Strunz and et al., "Benchmark Systems for Network Integration of Renewable and Distributed Energy Resources," CIGRÉ, Tech. Brochure 575, Apr. 2014.

[28] G. C. Kryonidis, C. S. Demoulias, and G. K. Papagiannis, "A two-stage solution to the bi-objective optimal voltage regulation problem," *IEEE Trans. Sustain. Energy*, vol. 11, no. 2, pp. 928–937, 2020.

[29] "European low voltage test feeder," Apr. 01, 2021. [Online]. [Online]. Available: https://site.ieee.org/pes-testfeeders/resources/

[30] PSIM, "Software by powersim technologies," *Professional Version*.

[31] G. C. Kryonidis, C. S. Demoulias, and G. K. Papagiannis, "A new voltage control scheme for active medium-voltage (mv) networks," *Electr. Power Syst. Res.*, vol. 169, pp. 53–64, 2019.

[32] K. D. Pippi, T. A. Papadopoulos, and G. C. Kryonidis, "Impact assessment framework of PV-BES systems to active distribution networks," *Med. Conf. Power Gen. Transm., Distrib. Energy Convers.*, pp. 1–6, 2020.